

---

# Hybrid Physical-Deep Learning Model for Astronomical Inverse Problems

---

**François Lanusse**

Berkeley Center for Cosmological Physics  
Berkeley Institute for Data Science  
University of California, Berkeley  
Berkeley, CA 94709  
flanusse@berkeley.edu

**Peter Melchior**

Department of Astrophysical Sciences  
Center for Statistics and Machine Learning  
Princeton University  
Princeton, NJ 08544, USA  
peter.melchior@princeton.edu

**Fred Moolekamp**

LSST Project Management Office  
Tucson, AZ, USA  
Department of Astrophysical Sciences  
Princeton University  
Princeton, NJ 08544, USA  
fredem@astro.princeton.edu

## Abstract

We present a Bayesian machine learning architecture that combines a physically motivated parametrization and an analytic error model for the likelihood with a deep generative model providing a powerful data-driven prior for complex signals. This combination yields an interpretable and differentiable generative model, allows the incorporation of prior knowledge, and can be utilized for observations with different data quality without having to retrain the deep network. We demonstrate our approach with an example of astronomical source separation in current imaging data, yielding a physical and interpretable model of astronomical scenes.

## 1 Introduction

Deep Learning is extremely efficient at solving a wide range of inverse problems, but what is gained in performance is often lost in interpretability due the black box nature of deep neural networks. In scientific applications however, the interpretability of the solution is often paramount, as is the ability to imbue pre-existing physical knowledge directly into the model. To this end, we propose an hybrid model based on solving for the Maximum A Posteriori (MAP) solution of an inverse problem, where a physical model is used to describe the forward data acquisition process, and a deep generative model with explicit likelihood is used to provide a complex data-driven signal prior.

**Related Work** With the success of deep learning in many classical imaging problems (e.g. Dong et al., 2016), a significant amount of effort has been aimed at linking deep learning successes back to the classical inverse problems literature. Several avenues have been explored, e.g. learning a denoiser as an implicit proximal operator (Meinhardt et al., 2017); using a generative model as deep image prior (Lempitsky et al., 2018); learning a convolutional dictionary and proximal operator (Yang et al., 2016); or learning implicitly both the prior and the inference algorithm itself (Putzky and Welling, 2017). Finally, most closely related to our work, (Dave et al., 2018) introduces the idea of modeling the prior explicitly at the pixel-level using a deep generative model.

## 2 Problem statement

We consider a general linear inverse problems of the form:

$$\mathbf{y} = \mathbf{A}\mathbf{x} + \mathbf{n}, \quad (1)$$

where  $\mathbf{y}$  are the observations,  $\mathbf{x}$  is the unknown signal to recover,  $\mathbf{A}$  is a linear degradation operator,  $\mathbf{n}$  is some observational noise. This problem describes a wide range of applications from MRI to radio-interferometry through different choices of the operator  $\mathbf{A}$ .

In the Bayesian approach to inverse problems, the posterior  $p(\mathbf{x}|\mathbf{y})$  can be expressed as

$$p(\mathbf{x}|\mathbf{y}) \propto p(\mathbf{y}|\mathbf{x}) p(\mathbf{x}). \quad (2)$$

- The *data likelihood* term  $p(\mathbf{y}|\mathbf{x})$  encodes our physical understanding of the forward process that leads to the observations. We assume here that for a given  $\mathbf{x}$ , this term can be evaluated explicitly given our physical model.
- The *prior* term  $p(\mathbf{x})$  encodes our prior knowledge on the solution we seek to recover. This prior can be informed by prior experiments, complementary data, or physical considerations. A tractable expression of this prior can often be obtained only for simple signal classes.

While the Bayesian solution to such inverse problem is the full posterior  $p(\mathbf{x}|\mathbf{y})$ , in many practical applications the full distribution is typically reduced to a single point estimate, i.e. the Maximum A Posteriori (MAP) solution

$$\mathbf{x}_{MAP} = \arg \max_x \log p(\mathbf{y}|\mathbf{x}) + \log p(\mathbf{x}). \quad (3)$$

We will exploit this separable representation, limiting the use of deep learning to the prior term  $p(\mathbf{x})$ .

**Model for the data likelihood** With a given operator  $\mathbf{A}$ , the likelihood term is completely characterized by the noise model for  $\mathbf{n}$ . We assume a Gaussian noise model, i.e.  $\mathbf{n} \sim \mathcal{N}(0, \Sigma)$  where  $\Sigma$  is the noise covariance. In this case  $\log p(\mathbf{y}|\mathbf{x}) = -\frac{1}{2}\|\mathbf{y} - \mathbf{A}\mathbf{x}\|_{\Sigma^{-1}}^2 + cst$ , where  $\|\mathbf{x}\|_{\mathbf{M}}^2 = \mathbf{x}^T \mathbf{M} \mathbf{x}$ .

**Deep generative models as complex data priors** Models like Variational AutoEncoders (VAEs) (Kingma and Welling, 2013) and Generative Adversarial Networks (GANs) (Goodfellow et al., 2014) have been extremely successful, but they do not provide an explicit likelihood  $p(\mathbf{x})$ . Instead we choose to rely on pixel autoregressive models (Oord et al., 2016; Salimans et al., 2017; Chen et al., 2018) which provide an explicit likelihood, factorized into separate conditional distributions  $p_{\theta}(\mathbf{x}) = \prod_i p_{\theta}(x_i|x_0 \dots x_{i-1})$  where  $\theta$  are the weights of the model. These models achieve state of the art performance, are stable during training, and do not suffer from mode collapse (contrary to GANs). Our prior model is trained on uncorrupted examples of data  $\mathbf{x}$ , which may come from simulations or from high-fidelity observations.

**Physical constraints as proximal regularization terms** In this approach, most of the prior information stems from the data-driven deep generative model  $p_{\theta}(\mathbf{x})$ . However, additional physical constraints on the solution can be applied by adding regularization terms to the prior:  $\log p(\mathbf{x}) = \log p_{\theta}(\mathbf{x}) + \sum_j R_j(\mathbf{x})$ . The regularizers may be non-differentiable as long as they can be expressed by their proximal operators  $\text{prox}_{R_j}(\mathbf{x})$ . As an example, the flux of astronomical sources is a positive quantity, we may therefore want to impose a non-negativity constraint  $\iota_{>0}(\mathbf{x})$  on the solution, using the associated proximal operator  $\text{prox}_{\iota_{>0}}(\mathbf{x}) = \max(0, \mathbf{x})$ .

Combining all these elements, we can characterize our  $\mathbf{x}_{MAP}$  solution as the minimum of the following loss function:

$$\mathcal{L} = \frac{1}{2}\|\mathbf{y} - \mathbf{A}\mathbf{x}\|_{\Sigma^{-1}}^2 - \log p_{\theta}(\mathbf{x}) + \sum_i R_i(\mathbf{x}) \equiv f(\mathbf{x}) + g(\mathbf{x}) + r(\mathbf{x}). \quad (4)$$

The two first components of this loss are differentiable and therefore amenable to gradient descent. Due to the presence of non-differentiable regularizers, the optimization makes use of the iterative Proximal Gradient Method (also known as forward-backward splitting (Combettes and Wajs, 2005))

$$\mathbf{x}_{t+1} = \underset{\lambda_t r}{\text{prox}}(\mathbf{x}_t - \lambda_t \nabla(f + g)(\mathbf{x}_t)), \quad (5)$$

which converges to a minimum of  $\mathcal{L}$  if the step size  $\lambda$  is smaller than  $2/L$ , where  $L$  is the Lipschitz constant of the gradient term.

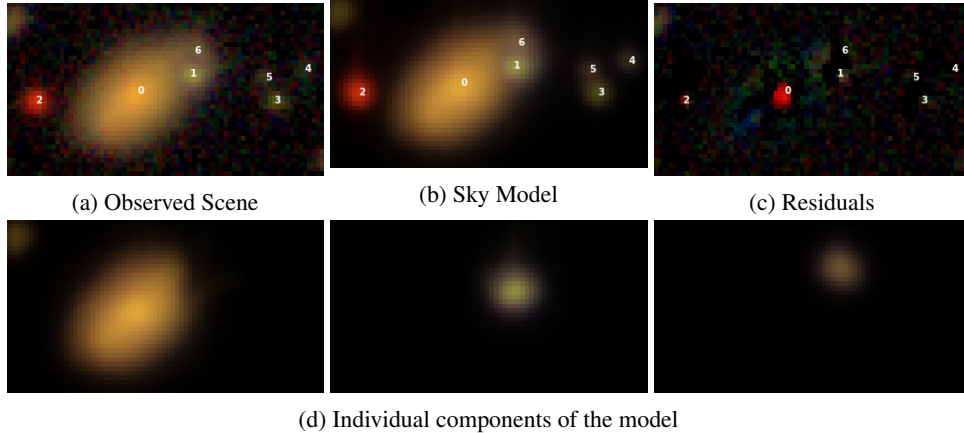


Figure 1: Deblending of a scene from the HSC imaging survey using the proposed model. The sky model (b), composed of individual sources (marked in white) with their own morphology and SED, is fitted to the observations (a). A subset of the individual recovered components are shown in (d).

### 3 Application: deblending galaxy images

Modern wide-field cosmological surveys cover large areas of the sky with ever increasing imaging quality (e.g. LSST Science Collaboration et al., 2009; Laureijs et al., 2011). They often seek to simultaneously address many scientific goals, e.g. mapping the large scale structure of the Universe to answer fundamental questions on the nature of Dark Matter and Dark Energy. One outstanding challenge faced by all modern imaging surveys is the overlap of several sources (stars and galaxies) on the sky, so-called "blending". It complicates the measurement of properties of individual members of the blend. This problem constitutes a typical instance of blind source separation, which attempts to separate all components of a blended scene without *a priori* knowledge of their nature (see Figure 1). A GAN-based approach to deblending was introduced in (Reiman and Göhre, 2019) but suffers from the typical limitations of black-box deep learning models, i.e. it cannot account for different observing conditions or noise levels without retraining the full model, is limited to separating two components, and has no test-time flux preservation.

We propose to address the deblending problem using the analytic model of the scene introduced by Melchior et al. (2018). Given an astronomical scene  $\mathbf{y} \in \mathbb{R}^{B \times N \times N}$  observed in  $B$  bands (i.e. using multiple filters), each source  $k$  in the scene is modeled with a non-parametric shape  $S_k \in \mathbb{R}^{N \times N}$  and an amplitude  $A_k \in \mathbb{R}^B$ , the so-called Spectral Energy Distribution (SED), which determines how bright the object will appear in each band. Multiple sources contribute additively to the scene, which is correct in the absence of absorbers, e.g. inter-stellar dust. The forward model also needs to account for degradation of the image caused by the atmosphere and the instrumental optics. This can be described as a band-wise 2D convolution by a Point Spread Function (PSF). We denote  $\mathbf{P}$  as block-diagonal linear operator implementing the convolution in each band by the appropriate PSF. It acts as the operator  $\mathbf{A}$  in Equation 1. Our full physical model for the scene can now be expressed as:

$$\mathbf{y} = \mathbf{P} \sum_{k=1}^K A_k^T \times S_k + \mathbf{n} \quad (6)$$

where  $\mathbf{n} \in \mathbb{R}^{B \times N \times N}$  is typically assumed to be Gaussian noise with covariance  $\Sigma$ . The deblending problem is to recover an estimate of both the morphology  $S_k$  and the SED  $A_k$  of each component of the blend, subject to additional constraints such as positivity of the source emission ( $S_k > 0$  and  $A_k > 0$ ). Applying the framework described in section 2, we solve the optimization problem

$$\arg \min_{S_k, A_k} \frac{1}{2} \|\mathbf{y} - \mathbf{P} \sum_{k=1}^K A_k^T \times S_k\|_{\Sigma^{-1}}^2 + \sum_k \log p_{\theta}(S_k) + \iota_{>0}(A_k) + \iota_{>0}(S_k), \quad (7)$$

by a block-wise application of Equation 5 to every optimization variable. We base the morphology prior  $p_{\theta}$  on the PixelCNN++ model (Salimans et al., 2017), which we adjust for continuous signals by using a simple Gaussian model for the conditional distribution  $p_{\theta}(x_i | x_0 \dots x_{i-1})$ . The prior  $p_{\theta}$  is trained on an existing set of high-resolution images of isolated galaxies (Mandelbaum et al., 2012,

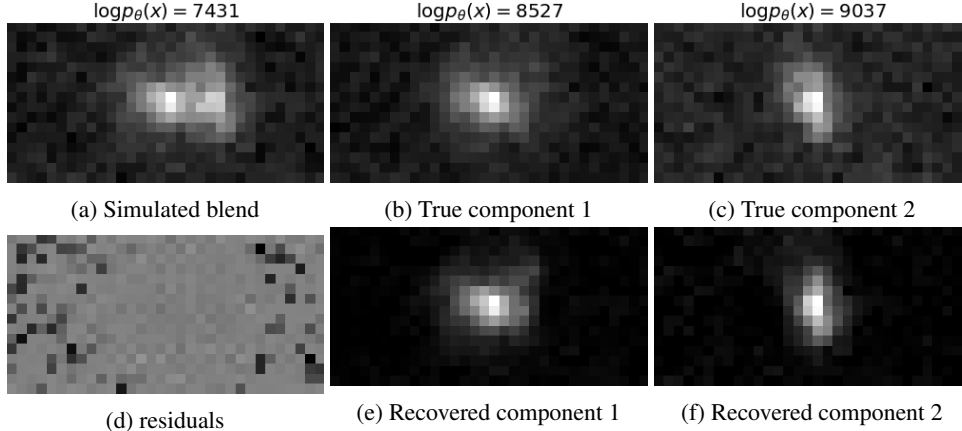


Figure 2: Artificial blend experiment, simulated from HST observations, demonstrating the ability of the prior to disentangle sources from their morphologies alone. The log likelihood evaluated on the trained prior for the blended and isolated sources is reported in the top row: a blended object (a) has lower log likelihood than isolated objects (b, c) under the prior. This allows us to separate (e) and (f) when given (a).

2014; Rowe et al., 2015) from the Hubble Space Telescope (HST)/Advanced Camera for Surveys (ACS) COSMOS survey (Koekemoer et al., 2007). These single-band high-resolution images from HST are reconvolved with a uniform reference PSF and resampled to match the pixel scale of the test survey, the Hyper Suprime-Cam (HSC) survey from the Subaru 8.2 meter telescope on Maunakea, Hawaii (Aihara et al., 2018). Figure 2b and Figure 2c show examples of two isolated galaxies obtained by this procedure, annotated with the log likelihood  $\log p_\theta(x)$  of the trained prior. Figure 2a shows a simulated blend obtained by adding these two isolated galaxies. The log likelihood under the prior for both galaxies combined is lower than for each isolated galaxy, demonstrating that the morphology prior provides information that can be leveraged for deblending.

Equipped with the prior on single-galaxy morphology, we tackle the blended scene in Figure 1 from the first public HSC data. The observations, made in  $B = 5$  different filters, are modelled with Equation 6, where the number of sources  $K$  and a first guess of their positions is provided by an external detection algorithm. We infer the parameters of the scene by solving Equation 7, yielding a sky model (Figure 1b) which can be separated into its individual components (Figure 1d). The model creates an excellent fit to morphologies and SEDs despite the strong overlap of several sources. The residuals are dominated by an undetected nuclear component in the brightest galaxy, which could be modeled by adding another component there. Finally, our model analytically accounts for different observing conditions. We provide in Appendix A a comparison to the state-of-the-art SCARLET deblender (Melchior et al., 2018) on this scene to highlight the benefits of the deep morphology prior. In Figure 3 we show the same blended scene, but we artificially increased the noise RMS by a factor of 3. By adjusting the noise covariance in Equation 7, the methods recovers a very similar result without the need to retrain the deep learning prior. We could also address e.g. additional blurring from a wider PSF or resampling to lower resolution with the same approach.

## 4 Conclusion

We have presented a hybrid Bayesian framework for inverse problems that combines analytic forward modeling for the likelihood with deep generative models for complex data-driven signal priors. This approach makes explicit use of physically motivated problem structure and prior knowledge from high-quality observations. When applied to the blind-source separation problem of galaxy blending, we can retrieve multi-components models of astronomical scenes that are by construction robust to changes in observational conditions.

## References

- Aihara, H., Arimoto, N., Armstrong, R., Arnouts, S., Bahcall, N. A., Bickerton, S., Bosch, J., Bundy, K., Capak, P. L., Chan, J. H. H., Chiba, M., Coupon, J., Egami, E., Enoki, M., Finet, F., Fujimori, H., Fujimoto, S., Furusawa, H., Furusawa, J., Goto, T., Goulding, A., Greco, J. P., Greene, J. E., Gunn, J. E., Hamana, T., Harikane, Y., Hashimoto, Y., Hattori, T., Hayashi, M., Hayashi, Y.,

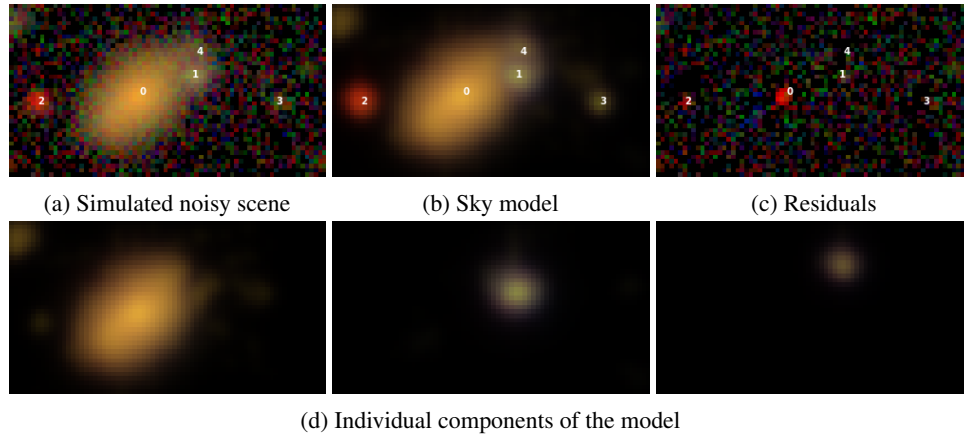


Figure 3: Same as Figure 1, but with artificially increased noise ( $\text{RMS} \times 3$ ).

Helminiak, K. G., Higuchi, R., Hikage, C., Ho, P. T. P., Hsieh, B.-C., Huang, K., Huang, S., Ikeda, H., Imanishi, M., Inoue, A. K., Iwasawa, K., Iwata, I., Jaelani, A. T., Jian, H.-Y., Kamata, Y., Karoji, H., Kashikawa, N., Katayama, N., Kawanomoto, S., Kayo, I., Koda, J., Koike, M., Kojima, T., Komiyama, Y., Konno, A., Koshida, S., Koyama, Y., Kusakabe, H., Leauthaud, A., Lee, C.-H., Lin, L., Lin, Y.-T., Lupton, R. H., Mandelbaum, R., Matsuoka, Y., Medezinski, E., Mineo, S., Miyama, S., Miyatake, H., Miyazaki, S., Momose, R., More, A., More, S., Moritani, Y., Moriya, T. J., Morokuma, T., Mukae, S., Murata, R., Murayama, H., Nagao, T., Nakata, F., Niida, M., Niikura, H., Nishizawa, A. J., Obuchi, Y., Oguri, M., Oishi, Y., Okabe, N., Okamoto, S., Okura, Y., Ono, Y., Onodera, M., Onoue, M., Osato, K., Ouchi, M., Price, P. A., Pyo, T.-S., Sako, M., Sawicki, M., Shibuya, T., Shimasaku, K., Shimono, A., Shirasaki, M., Silverman, J. D., Simet, M., Speagle, J., Spergel, D. N., Strauss, M. A., Sugahara, Y., Sugiyama, N., Suto, Y., Suyu, S. H., Suzuki, N., Tait, P. J., Takada, M., Takata, T., Tamura, N., Tanaka, M. M., Tanaka, M., Tanaka, M., Tanaka, Y., Terai, T., Terashima, Y., Toba, Y., Tominaga, N., Toshikawa, J., Turner, E. L., Uchida, T., Uchiyama, H., Umetsu, K., Uruguchi, F., Urata, Y., Usuda, T., Utsumi, Y., Wang, S.-Y., Wang, W.-H., Wong, K. C., Yabe, K., Yamada, Y., Yamanoi, H., Yasuda, N., Yeh, S., Yonehara, A., and Yuma, S. (2018). The Hyper Suprime-Cam SSP Survey: Overview and survey design. *Publications of the Astronomical Society of Japan*, 70(SP1):1–5.

Chen, X., Mishra, N., Rohaninejad, M., and Abbeel, P. (2018). PixelSNAIL: An improved autoregressive generative model. *35th International Conference on Machine Learning, ICML 2018*, 2:1364–1372.

Combettes, P. L. and Wajs, V. R. (2005). Signal Recovery by Proximal Forward-Backward Splitting. *Multiscale Modeling & Simulation*, 4(4):1168–1200.

Dave, A., Vadathya, A. K., Subramanyam, R., Baburajan, R., and Mitra, K. (2018). Solving Inverse Computational Imaging Problems Using Deep Pixel-Level Prior. *IEEE Transactions on Computational Imaging*, 5(1):37–51.

Dong, C., Loy, C. C., He, K., and Tang, X. (2016). Image Super-Resolution Using Deep Convolutional Networks. *IEEE Transactions on Pattern Analysis and Machine Intelligence*, 38(2):295–307.

Goodfellow, I., Pouget-Abadie, J., and Mirza, M. (2014). Generative Adversarial Networks. *arXiv preprint arXiv: ...*, pages 1–9.

Kingma, D. P. and Welling, M. (2013). Auto-Encoding Variational Bayes. 587(MI).

Koekemoer, A., Aussel, H., Calzetti, D., Capak, P., Giavalisco, M., Kneib, J.-P., Leauthaud, A., Le Fèvre, O., Mccracken, H., Massey, R., Mobasher, B., Rhodes, J., Scoville, N., and Shopbell, P. (2007). The COSMOS survey: Hubble Space Telescope Advanced Camera for Surveys observations and data processing. *Astrophysical Journal, Supplement Series*, 172(1):196–202.

Laureijs, R., Amiaux, J., Arduini, S., Augueres, J. L., Brinchmann, J., Cole, R., Cropper, M., Dabin, C., Duvet, L., Ealet, A., Garilli, B., Gondoin, P., Guzzo, L., Hoar, J., Hoekstra, H., Holmes, R., Kitching, T., Maciaszek, T., Mellier, Y., Pasian, F., Percival, W., Rhodes, J., Saavedra Criado, G., Sauvage, M., Scaramella, R., Valenziano, L., Warren, S., Bender, R., Castander, F., Cimatti, A., Le Fevre, O., Kurki-Suonio, H., Levi, M., Lilje, P., Meylan, G., Nichol, R., Pedersen, K., Popa, V., Rebolo Lopez, R., Rix, H. W., Rottgering, H., Zeilinger, W., Grupp, F., Hudelot, P., Massey, R., Meneghetti, M., Miller, L., Paltani, S., Paulin-Henriksson, S., Pires, S., Saxton, C., Schrabback, T., Seidel, G., Walsh, J., Aghanim, N., Amendola, L., Bartlett, J., Baccigalupi, C., Beaulieu, J. P., Benabed, K., Cuby, J. G., Elbaz, D., Fosalba, P., Gavazzi, G., Helmi, A., Hook, I., Irwin, M., Kneib, J. P., Kunz, M., Mannucci, F., Moscardini, L., Tao, C., Teyssier, R., Weller, J., Zamorani, G., Zapatero Osorio, M. R., Boulade, O., Foumond, J. J., Di Giorgio, A., Guttridge, P., James, A., Kemp, M., Martignac, J., Spencer, A., Walton, D., Blumchen, T., Bonoli, C., Bortoletto, F., Cerna, C., Corcione, L., Fabron, C., Jahnke, K., Ligi, S., Madrid, F., Martin, L., Morgante, G., Pamplona, T., Prieto, E., Riva, M., Toledo, R., Trifoglio, M., Zerbi, F., Abdalla, F., Douspis, M., Grenet, C., Borgani, S., Bouwens, R., Courbin, F., Delouis, J. M., Dubath, P., Fontana, A., Frailis, M., Grazian, A., Koppenhofer, J., Mansutti, O., Melchior, M., Mignoli, M., Mohr, J., Neissner, C., Noddle, K., Poncet, M., Scodreggio, M., Serrano, S., Shane, N., Starck, J. L., Surace, C., Taylor, A., Verdoes-Kleijn, G., Vuerli, C., Williams, O. R., Zacchei, A., Altieri, B., Escudero Sanz, I., Kohley, R., Oosterbroek, T., Astier, P., Bacon, D., Bardelli, S., Baugh, C., Bellagamba, F., Benoist, C., Bianchi, D., Biviano, A., Branchini, E., Carbone, C., Cardone, V., Clements, D., Colombi, S., Conselice, C., Cresci, G., Deacon, N., Dunlop, J., Fedeli, C., Fontanot, F., Franzetti, P., Giocoli, C., Garcia-Bellido, J., Gow, J., Heavens, A., Hewett, P., Heymans, C., Holland, A., Huang, Z., Ilbert, O., Joachimi, B., Jennins, E., Kerins, E., Kiessling, A., Kirk, D., Kotak, R., Krause, O., Lahav, O., van Leeuwen, F., Lesgourgues, J., Lombardi, M., Magliocchetti, M., Maguire, K., Majerotto, E., Maoli, R., Marulli, F., Maurogordato, S., McCracken, H., McLure, R., Melchiorri, A., Merson, A., Moresco, M., Nonino, M., Norberg, P., Peacock, J., Pello, R., Penny, M., Pettorino, V., Di Porto, C., Pozzetti, L., Quercellini, C., Radovich, M., Rassat, A., Roche, N., Ronayette, S., Rossetti, E., Sartoris, B., Schneider, P., Semboloni, E., Serjeant, S., Simpson, F., Skordis, C., Smadja, G., Smartt, S., Spano, P., Spiro, S., Sullivan, M., Tilquin, A., Trotta, R., Verde, L., Wang, Y., Williger, G., Zhao, G., Zoubian, J., and Zucca, E. (2011). Euclid Definition Study Report. *ArXiv e-prints*, page arXiv:1110.3193.

Lempitsky, V., Vedaldi, A., and Ulyanov, D. (2018). Deep Image Prior. *Proceedings of the IEEE Computer Society Conference on Computer Vision and Pattern Recognition*, pages 9446–9454.

LSST Science Collaboration, Abell, P. A., Allison, J., Anderson, S. F., Andrew, J. R., Angel, J. R. P., Armus, L., Arnett, D., Asztalos, S. J., Axelrod, T. S., Bailey, S., Ballantyne, D. R., Bankert, J. R., Barkhouse, W. A., Barr, J. D., Barrientos, L. F., Barth, A. J., Bartlett, J. G., Becker, A. C., Becla, J., Beers, T. C., Bernstein, J. P., Biswas, R., Blanton, M. R., Bloom, J. S., Bochanski, J. J., Boeshaar, P., Borne, K. D., Bradac, M., Brandt, W. N., Bridge, C. R., Brown, M. E., Brunner, R. J., Bullock, J. S., Burgasser, A. J., Burge, J. H., Burke, D. L., Cargile, P. A., Chandrasekharan, S., Chartas, G., Chesley, S. R., Chu, Y.-H., Cinabro, D., Claire, M. W., Claver, C. F., Clowe, D., Connolly, A. J., Cook, K. H., Cooke, J., Cooray, A., Covey, K. R., Culliton, C. S., de Jong, R., de Vries, W. H., Debattista, V. P., Delgado, F., Dell’Antonio, I. P., Dhital, S., Di Stefano, R., Dickinson, M., Dilday, B., Djorgovski, S. G., Dobler, G., Donalek, C., Dubois-Felsmann, G., Durech, J., Eliasdottir, A., Eracleous, M., Eyer, L., Falco, E. E., Fan, X., Fassnacht, C. D., Ferguson, H. C., Fernandez, Y. R., Fields, B. D., Finkbeiner, D., Figueroa, E. E., Fox, D. B., Francke, H., Frank, J. S., Frieman, J., Fromenteau, S., Furqan, M., Galaz, G., Gal-Yam, A., Garnavich, P., Gawiser, E., Geary, J., Gee, P., Gibson, R. R., Gilmore, K., Grace, E. A., Green, R. F., Gressler, W. J., Grillmair, C. J., Habib, S., Haggerty, J. S., Hamuy, M., Harris, A. W., Hawley, S. L., Heavens, A. F., Hebb, L., Henry, T. J., Hileman, E., Hilton, E. J., Hoadley, K., Holberg, J. B., Holman, M. J., Howell, S. B., Infante, L., Ivezić, Z., Jacoby, S. H., Jain, B., R. Jedicke, Jee, M. J., Jernigan, J. G., Jha, S. W., Johnston, K. V., Jones, R. L., Juric, M., Kaasalainen, M., Styliani, Kafka, Kahn, S. M., Kaib, N. A., Kalirai, J., Kantor, J., Kasliwal, M. M., Keeton, C. R., Kessler, R., Knezevic, Z., Kowalski, A., Krabbendam, V. L., Krughoff, K. S., Kulkarni, S., Kuhlman, S., Lacy, M., Lepine, S., Liang, M., Lien, A., Lira, P., Long, K. S., Lorenz, S., Lotz, J. M., Lupton, R. H., Lutz, J., Macri, L. M., Mahabal, A. A., Mandelbaum, R., Marshall, P., May, M., McGehee, P. M., Meadows, B. T., Meert, A., Milani, A., Miller, C. J., Miller, M., Mills, D., Minniti, D., Monet, D., Mukadam, A. S., Nakar, E., Neill, D. R., Newman, J. A., Nikolaev, S., Nordby, M., O’Connor, P., Oguri, M., Oliver, J., Olivier, S. S., Olsen, J. K., Olsen, K., Olszewski, E. W., Oluseyi, H., Padilla, N. D., Parker, A.,

- Pepper, J., Peterson, J. R., Petry, C., Pinto, P. A., Pizagno, J. L., Popescu, B., Prsa, A., Radcka, V., Raddick, M. J., Rasmussen, A., Rau, A., Rho, J., Rhoads, J. E., Richards, G. T., Ridgway, S. T., Robertson, B. E., Roskar, R., Saha, A., Sarajedini, A., Scannapieco, E., Schalk, T., Schindler, R., Schmidt, S., Schmidt, S., Schneider, D. P., Schumacher, G., Scranton, R., Sebag, J., Seppala, L. G., Shemmer, O., Simon, J. D., Sivertz, M., Smith, H. A., Smith, J. A., Smith, N., Spitz, A. H., Stanford, A., Stassun, K. G., Strader, J., Strauss, M. A., Stubbs, C. W., Sweeney, D. W., Szalay, A., Szkody, P., Takada, M., Thorman, P., Trilling, D. E., Trimble, V., Tyson, A., Van Berg, R., Berk, D. V., VanderPlas, J., Verde, L., Vrsnak, B., Walkowicz, L. M., Wandelt, B. D., Wang, S., Wang, Y., Warner, M., Wechsler, R. H., West, A. A., Wiecha, O., Williams, B. F., Willman, B., Wittman, D., Wolff, S. C., Wood-Vasey, W. M., Wozniak, P., Young, P., Zentner, A., and Zhan, H. (2009). LSST Science Book, Version 2.0. *arXiv.org*, astro-ph.I(November):201.
- Mandelbaum, R., Lackner, C., Leauthaud, A., and Rowe, B. (2012). COSMOS real galaxy dataset.
- Mandelbaum, R., Rowe, B., Bosch, J., Chang, C., Courbin, F., Gill, M., Jarvis, M., Kannawadi, A., Kacprzak, T., Lackner, C., Leauthaud, A., Miyatake, H., Nakajima, R., Rhodes, J., Simet, M., Zuntz, J., Armstrong, B., Bridle, S., Coupon, J., Dietrich, J. P., Gentile, M., Heymans, C., Jurling, A. S., Kent, S. M., Kirkby, D., Margala, D., Massey, R., Melchior, P., Peterson, J., Roodman, A., and Schrabback, T. (2014). The Third Gravitational Lensing Accuracy Testing (GREAT3) Challenge Handbook. *The Astrophysical Journal Supplement Series*, 212(1):5.
- Meinhardt, T., Möller, M., Hazirbas, C., and Cremers, D. (2017). Learning Proximal Operators: Using Denoising Networks for Regularizing Inverse Imaging Problems. (October).
- Melchior, P., Moolekamp, F., Jerdee, M., Armstrong, R., Sun, A.-L., Bosch, J., and Lupton, R. (2018). scarlet : Source separation in multi-band images by Constrained Matrix Factorization. *Astronomy and Computing*, 24:129–142.
- Oord, A. v. d., Kalchbrenner, N., and Kavukcuoglu, K. (2016). Pixel Recurrent Neural Networks. *International Conference on Machine Learning (ICML)*, 48.
- Putzky, P. and Welling, M. (2017). Recurrent Inference Machines for Solving Inverse Problems. (Nips).
- Reiman, D. M. and Göhre, B. E. (2019). Deblending galaxy superpositions with branched generative adversarial networks. *Monthly Notices of the Royal Astronomical Society*, 485(2):2617–2627.
- Rowe, B. T. P., Jarvis, M., Mandelbaum, R., Bernstein, G. M., Bosch, J., Simet, M., Meyers, J. E., Kacprzak, T., Nakajima, R., Zuntz, J., Miyatake, H., Dietrich, J. P., Armstrong, R., Melchior, P., and Gill, M. S. S. (2015). GalSim: The modular galaxy image simulation toolkit. *Astronomy and Computing*, 10:121–150.
- Salimans, T., Karpathy, A., Chen, X., and Kingma, D. P. (2017). PixelCNN++: Improving the PixelCNN with Discretized Logistic Mixture Likelihood and Other Modifications. pages 1–10.
- Yang, Y., Sun, J., Li, H., and Xu, Z. (2016). Deep ADMM-Net for compressive sensing MRI. *Advances in Neural Information Processing Systems*, (Nips):10–18.

## A Comparison to the SCARLET deblender

In this appendix, we compare the proposed method with the baseline deblending algorithm SCARLET, which constitutes a state-of-the-art deblender for ground-based images (Melchior et al., 2018). SCARLET uses the same parameterization and loss function; in fact the work described here uses the same code base and only differs in the assumptions about galaxy morphologies.

In its default configuration, SCARLET assumes every  $S_k$  to be non-negative, symmetric under rotation of  $180^\circ$  and monotonically decreasing away from the center. These hard constraints can directly be enforced through proximal mappings in Equation 4 and have been found successful as regularizers of the deblending problem for ground-based images. They do not perform well on complex and irregular galaxies, which is the original motivation for the present work: replacing analytic, heuristic constraints by a data-driven deep morphology prior.

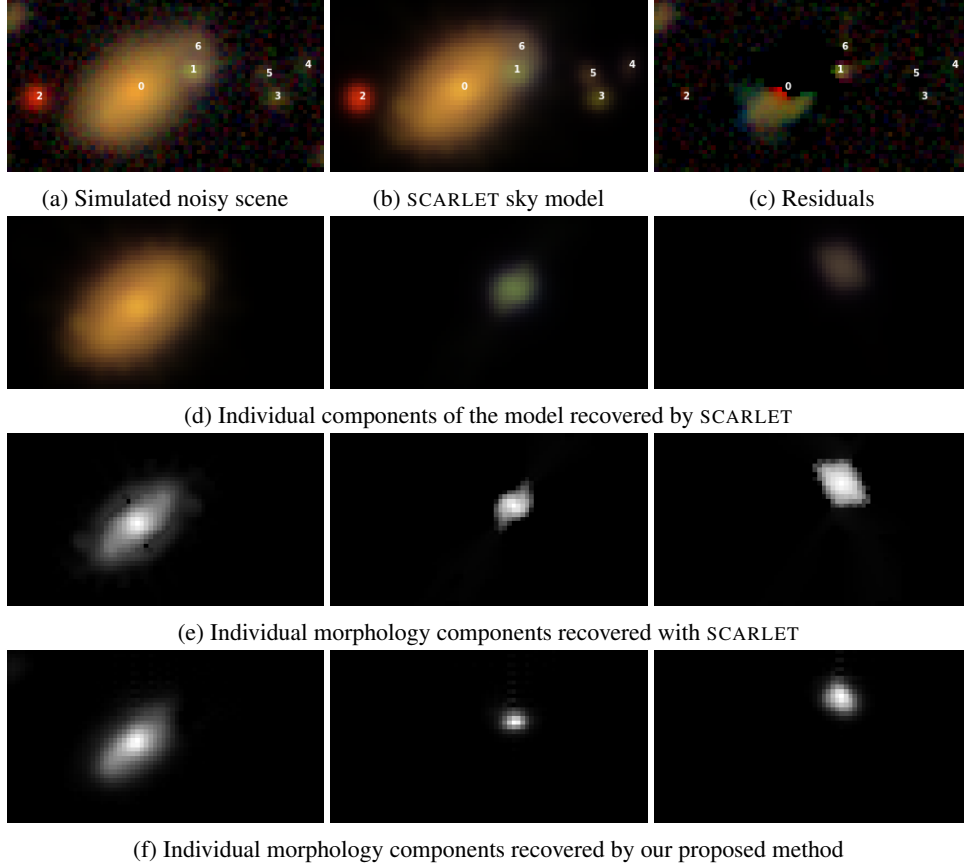


Figure 4: Similar to Figure 1, but using the deblender SCARLET with default settings. We also compare in (e) and (f) the deconvolved morphology components ( $S_k$  in Equation 6) recovered using the strict monotonicity and symmetry constraints in SCARLET with the deep morphology priors from this work.

Figure 4 show the result of running baseline SCARLET on the same data set. The residuals are significantly larger than in Figure 2 due to the inadequacies of the strict symmetry and monotonicity assumptions. This can also be seen by directly comparing the recovered deconvolved morphologies (lower panels of Figure 4). The symmetry constraint can lead to artifacts in the direction of a nearby source, in this example the model of source 0 is influenced by source 1. The morphologies recovered under the deep morphology prior are by construction realistic and do not exhibit such obvious artifacts.

While this comparison remains qualitative, it illustrates that the deep morphology prior addresses one main limitation of the SCARLET algorithm. A thorough study of our extension for the science cases of the upcoming LSST survey (LSST Science Collaboration et al., 2009) will be the main focus of an upcoming science paper geared towards the astronomical community.